Nanotechnology **19** (2008) 495101 (10pp) doi:10.1088/0957-4484/19/49/495101

Facile biosynthesis, separation and conjugation of gold nanoparticles to doxorubicin

S Anil Kumar[1,2], **Yves-Alain Peter**[1] **and Jay L Nadeau**[2,3]

[1] Engineering Physics Department, École Polytechnique de Montréal, Montréal, QC H3C 3A7, Canada
[2] Department of Biomedical Engineering, McGill University, Montréal, QC H3A 2B4, Canada

E-mail: jay.nadeau@mcgill.ca

Received 1 July 2008, in final form 26 September 2008
Published 18 November 2008
Online at stacks.iop.org/Nano/19/495101

Abstract
Particle shape and size determine the physicochemical and optoelectronic properties of nanoscale materials, including optical absorption, fluorescence, and electric and magnetic moments. It is thus desirable to be able to synthesize and separate various particle shapes and sizes. Biosynthesis using microorganisms has emerged as a more ecologically friendly, simpler, and more reproducible alternative to chemical synthesis of metal and semiconductor nanoparticles, allowing the generation of rare forms such as triangles. Here we show that the plant pathogenic fungus *Helminthosporum solani*, when incubated with an aqueous solution of chloroaurate ions, produces a diverse mixture of extracellular gold nanocrystals in the size range from 2 to 70 nm. A plurality are polydisperse spheres, but a significant number are homogeneously sized rods, triangles, pentagons, pyramids, and stars. The particles can be separated according to their size and shape by using a sucrose density gradient in a tabletop microcentrifuge, a novel and facile approach to nanocrystal purification. Conjugation to biomolecules can be performed without further processing, as illustrated with the smallest fraction of particles which were conjugated to the anti-cancer drug doxorubicin (Dox) and taken up readily into HEK293 cells. The cytotoxicity of the conjugates was comparable to that of an equivalent concentration of Dox.

S Supplementary data are available from stacks.iop.org/Nano/19/495101

(Some figures in this article are in colour only in the electronic version)

1. Introduction

The size- and shape-dependent properties of semiconductor and metal nanoparticles that arise from quantum confinement create materials qualitatively different from the bulk [10, 1]. Tremendous interest has been generated in the possibility of using these properties for biomedical targeting and labeling applications. The greatest barriers to biological use are issues of particle stability in water [33], toxicity [18], and shape and size control [44]. Colloidal chemical synthesis methods have produced an impressive range of homogeneously size-distributed forms: rods and wires [35, 17], cubes [39], triangles [6], disks [17], and arrows and tetrapods [32]. Challenging forms such as triangular pyramids have also been obtained using shape transformation [23], seeded growth [6], or annealing [8]. However, these methods are complex and often variable from experiment to experiment, and the resulting crystals are often poorly compatible with water and/or biological cells.

An alternative may be sought in biological methods of synthesis [4]. Microbial synthesis of metal [11, 38] and semiconductor [41, 12, 9] nanoparticles has been widely reported, resulting from the microorganisms' intrinsic metal-resistance mechanisms. Advantages of these methods include tightly controlled, highly reproducible syntheses; the generation of water-soluble, biocompatible particles; and the avoidance of toxic surfactants or organic solvents.

[3] Author to whom any correspondence should be addressed.

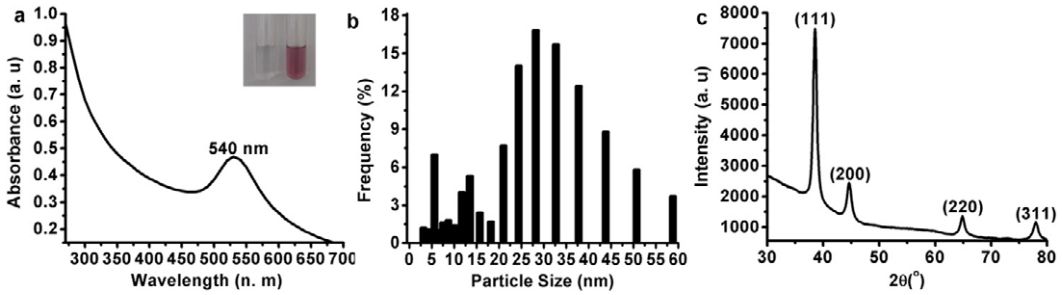

Figure 1. UV–vis spectra, dynamic light-scattering measurements and XRD of gold nanoparticles formed by the reaction of $AuCl_4^-$ with fungal biomass. (a) UV–vis spectra recorded from the external medium after 72 h. The inset shows test tubes containing the reaction mixture before (tube on the left, time 0) and after formation of gold nanoparticles (tube on the right, 72 h). (b) Dynamic light-scattering particle-size histogram of the solution after 72 h. (c) XRD analysis of the gold nanoparticles on a Si(111) wafer. The principal Bragg reflections are identified.

Disadvantages include lack of control over the resulting shapes and sizes, and often embedding of the particles within the cell matrix, necessitating extraction [40, 11]. A solution to both of these issues is to isolate the enzymes or other proteins responsible for the synthesis and to add them to the reaction mixture under variable conditions, as has been done to create elongated Au nanoparticles with *Escherichia coli* gold-binding enzymes [5] and spherical Au nanoparticles using fungal reductases [27, 28].

Here we use the plant pathogenic fungus, *Helminthosporum solani*, which when seeded with chloroaurate ions ($AuCl_4^-$) generates a mixture of different shapes of gold nanocrystallites in the size range from 2 to 70 nm. The particles are extracellular, requiring no purification apart from filtration. We also demonstrate the efficiency of a very simple sucrose density gradient technique to separate the mixture of biosynthesized gold nanoparticles based on their size and shape. Sucrose gradient is a technique commonly used to separate viruses and organelles by ultracentrifugation; it was reported once as a method for separating polymer nanoparticles [36]. In our application, the density of the particles permits separation with low speeds in a tabletop centrifuge.

The separated particles were hydrophilic, and we demonstrated bioconjugation by linking the smallest size fractions (∼2–5 nm) to doxorubicin via carbodiimide-mediated cross-linking. Doxorubicin is an anti-cancer drug that has been shown to be more effective when conjugated to hydrophilic nanoparticles that penetrate more deeply into the cell than the drug alone; nanoparticles may also enhance uptake of unbound doxorubicin [34, 16, 13, 43]. A quantum-dot based conjugate was recently developed that shows a fluorescent signal when doxorubicin is released into the cell [2]. Conjugates of gold nanoparticles to doxorubicin have not yet been reported, although gold particles have been FDA approved for human use and thus represent a promising vehicle for delivery of cytotoxic agents. Apart from being of low toxicity, gold particles have the advantage of providing CT contrast [25] and in serving as strong infrared absorbers for hyperthermic therapy [42, 21]. We show that conjugates were taken up into cell lines in a pattern very different from that of unbound doxorubicin, and could be visualized by both fluorescence and reflectance microscopy.

2. Experimental methods

Helminthosporum solani was maintained on PDA Petri dishes (potato 20% w/v, dextrose 2% w/v and agar 2% w/v) at 25 °C. Fermentation was carried out by inoculating a 1 cm diameter mycelium from a 7 day old PDA Petri dish into 100 ml liquid MGYP medium (0.3% w/v malt extract, 1.0% w/v glucose, 0.3% w/v, yeast extract and 0.5% w/v peptone) in a 500 ml Erlenmeyer flask, followed by incubation at 37 ± 1 °C on a rotary shaker (200 rpm) for 96 h. After the fermentation period, the mycelia were collected by centrifugation (5000 g, 15 °C, 20 min), washed thoroughly with distilled water under sterile conditions, and 20 g was suspended in 100 ml of 1 mM aqueous $AuCl_4$ solution in a 500 ml Erlenmeyer flask. The culture was then incubated at 37 ± 1 °C under shaking (200 rpm). Bioreduction was monitored by recording the UV–vis absorption spectra as a function of time of the reaction mixture. After saturation of the reaction process (found to be 72 h), the reaction mixture was filtered using a sterile 0.2 μM syringe filter.

Separation of the nanoparticles was achieved by creating a discontinuous sucrose density gradient by layering successively dilute sucrose solutions upon one another. This was done for small volumes in a 2 ml eppendorf centrifuge tube: 0.3 ml each of 30%, 40%, 50%, 60% and 70% w/v sucrose. The tube was marked in increments of single percentage points within each region. Finally 0.3 ml of the gold nanoparticle mixture was loaded onto this gradient in ddH_2O and centrifuged at 5000 g for 15 min in a microcentrifuge (Thermo Electron Corporation). Fractions (0.1 ml, representing approximately 3.3% increments) of the gradient were collected using a micropipette and characterized by TEM. For characterization of the larger particles by UV–vis spectroscopy, larger volumes were required. In this case, 6 ml each of 30%, 40%, 50%, 60% and 70% w/v sucrose were used in a 40 ml polystyrene centrifuge tube, 6 ml of the gold nanoparticle mixture was loaded onto this gradient, and the mixture centrifuged at 5000 g for 30 min in an IEC Centra-8R centrifuge (International Equipment Co., MA). 2 ml fractions were collected and further concentrated by first dialyzing against Milli Q water then concentrating to half of their volumes using a Speed Vac SC 100 (Savant Instruments, Minnesota, USA). For the largest particles, this step was repeated 2–3 times.

The concentration of each fraction was estimated from UV–vis spectra according to published methods [14]. Given the particle size known by TEM, concentration of particles smaller than 35 nm was estimated using the absorbance at 450 nm.

The smallest Au nanoparticle fractions (∼2–5 nm) obtained after sucrose density gradient were functionalized to doxorubicin by using the activator 1-ethyl-3-(3dimethylaminopropyl)-carbodiimide (EDC). The reaction was carried out in a 500 μl volume of 50 mM MES/HEPES buffer containing 30 μM of doxorubicin and varying concentrations of Au nanoparticles (0.25, 0.5 and 1 μM) to which 5 mM EDC was added. Conjugation was performed at 30 °C for 1 h, then unconjugated doxorubicin was removed by dialyzing the sample versus 1 l of 20 mM phosphate buffer (pH 7.2) containing 150 mM NaCl. The purified sample was further characterized by UV–vis and fluorescence spectroscopy and TEM. The number of Dox/Au particle was estimated by assuming no Au particles were lost in dialysis, and taking the Dox concentration after dialysis as $A(480)/\varepsilon$, where $\varepsilon = 11\,480\ \mathrm{M}^{-1}\ \mathrm{cm}^{-1}$ [26].

HEK293T cells were cultured in high-glucose DMEM (Invitrogen Canada, Burlington, ON) supplemented with L-glutamine (0.2 mM), penicillin (100 U ml^{-1}), streptomycin (100 μg ml^{-1}), and FBS (10%), and incubated in a 5% CO_2 humidified atmosphere. Cells were passaged onto glass-bottomed dishes (MatTek, Ashland, OR) 24–72 h before use. Conjugates were added to a final concentration of 10 nM gold particles and incubated for 1 h, then washed three times in PBS and observed. Control cells were incubated with 30 μM doxorubicin alone under the same conditions. Imaging was performed with an Olympus IX70 inverted fluorescence microscope equipped with a Nuance multispectral imaging system (including a visible liquid-crystal filter tunable between 420 and 750) (Cambridge Research Instruments). Epifluorescence illumination was through a quantum-dot filter cube set (excitation = 380–460 nm, dichroic 475 nm, emission = 500 longpass (LP); Chroma filter 32013).

Confocal microscopy was performed on cells after fixation for 30 min in 3.7% paraformaldehyde. Images were recorded on a Zeiss LSM 510 confocal laser scanning microscope using a PlanApo 100× objective. Simultaneous reflectance and fluorescence channels were used for all images; the fluorescent channel was an Ar laser line (488 nm) and 560 LP emission filter. Reflectance was obtained with a HeNe laser (543 nm) and a 535–590 bandpass output filter.

UV–vis absorbance spectra were recorded on a Spectra Max Plus plate reader (Molecular devices, Novato, CA) operated at a resolution of 1 nm. Dynamic light-scattering measurements were performed on a Zetasizer 5000 (Malvern Instruments) equipped with a He–Ne laser (633 nm, 5 mW), a photomultiplier detector and a Malvern 7132 Multibit autocorrelator. For x-ray diffraction (XRD), films of gold nanoparticles were prepared on Si(111) substrates by drop-coating. XRD was performed on the films with a Discover D8 x-ray diffractometer with a Xe/Ar gas filled Hi-Star area detector and a XYZ platform, operated at 40 kV and a current of 40 mA with Cu Kα radiation. A laser video system was

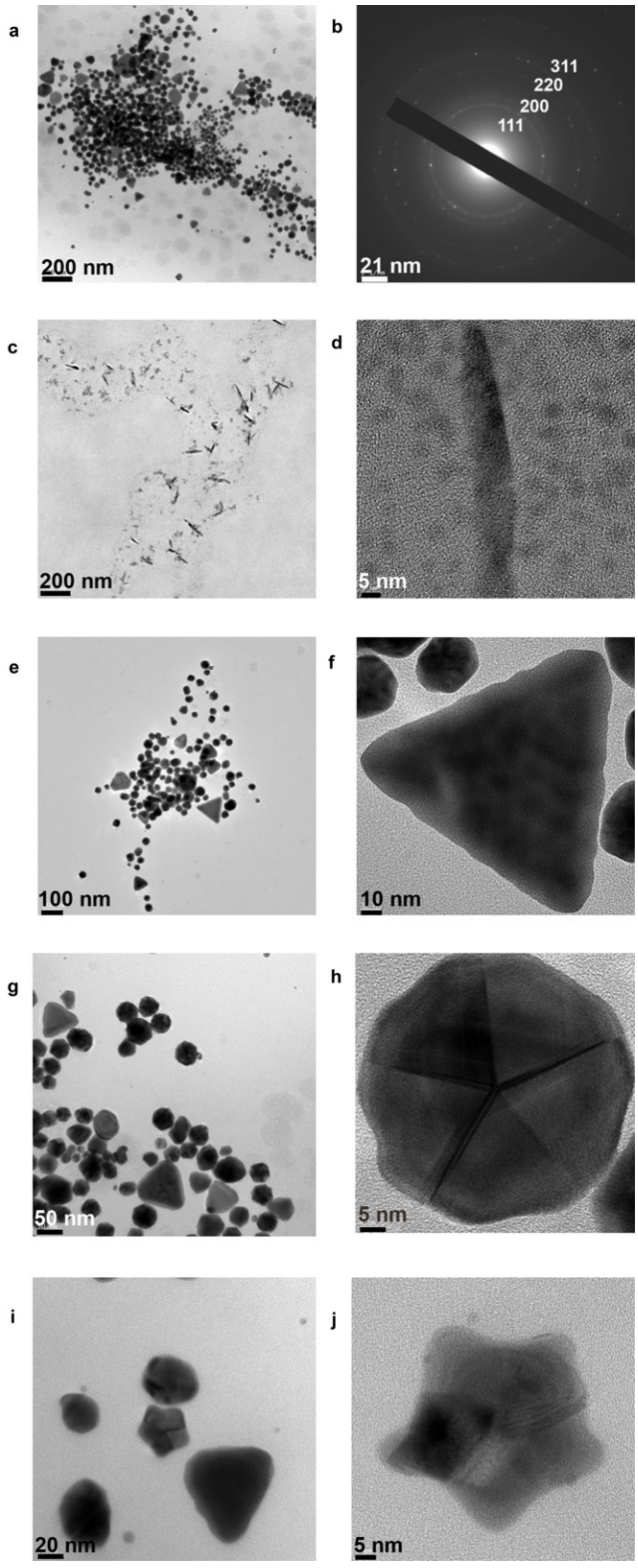

Figure 2. TEM analysis of the various shapes of gold nanoparticles formed after the reaction of $AuCl_4^-$ with fungal biomass. All images were taken before separation. (a) Mixture of all. (b) SAED pattern from one of the particles in (a). (c) Rod-shaped particles. (d) Higher magnification image of one of the rods. (e) Triangular particles. (f) Higher magnification image of one of the triangles. (g) Hexagonal particles. (h) Higher magnification image of one of the hexagons. (i) Star-shaped particles. (j) Higher magnification image of one of the stars.

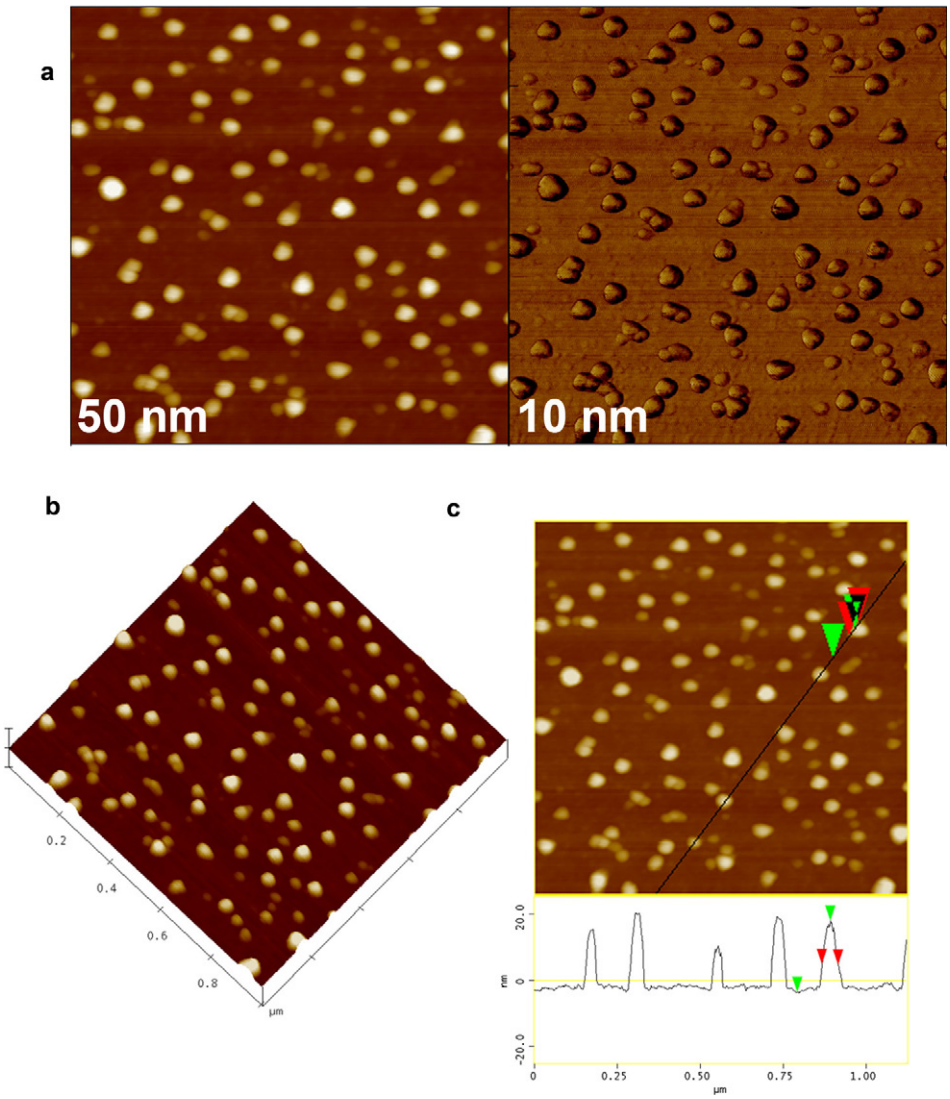

Figure 3. AFM images of the gold nanoparticles. (a) Topographical image. (b) Three-dimensional view. (c) Surface height and length profile of a selected set (black line) of the triangular nanoparticles seen in (b). The arrows indicate the precise points of the profile for a selected particle whose parameters are given in the text.

used to optically align the sample with the incident XRD beam. Samples for TEM were prepared on a carbon coated copper TEM grids. TEM measurements were performed on a JEOL Model 2100F EX transmission electron microscope operated at an accelerating voltage of 200 kV. For AFM, samples were prepared by spreading the nanoparticle solution onto a freshly cleaved mica (grade II) substrate and the solvent was dried using a nitrogen stream. AFM in the intermittent contact mode was performed using an enviroscope scanning probe microscope equipped with a Nanoscope III A controller from VEECO Digital Instruments, Santa Barbara, CA. AFM tips used were model Arrow-NCR etched Si tip at a resonance frequency of ∼300 kHz.

The MTT assay was performed using HEK293 cells seeded at 5×10^3 per well in a 96-well tissue culture plate. The cells were grown to 80% confluency, washed with PBS and incubated with different concentrations of Dox alone, Au alone, or Au–Dox for 1 h. Each treatment was performed in octuplet and the assay was repeated three times to ensure reproducibility. After exposure the cells were rinsed once with PBS, 200 μl of supplemented DMEM was added and the plate was incubated at 37 °C for 18–24 h. The MTT reagent (3-(4,5-dimethylthiazol-2-yl)-2,5-diphenyl tetrazolium bromide) was then added to each well (12.5 μl from 4 mg ml^{-1}) and the cells were incubated for 4 h. A final wash with PBS was performed, the PBS was aspirated and 200 μl of DMSO was added to each well, and absorbance was read at 560 nm.

3. Results and discussion

It has been shown previously that microscopic fungi can generate extracellular Au nanoparticles by a process involving NADH-reductases [27, 28] secreted by the cells under metal stress. We found that when aqueous chloroauric acid was added to an actively growing culture of the fungus *Helminthosporum solani*, the medium turned from colorless to red-purple over a time course of 72 h. Ultraviolet–visible

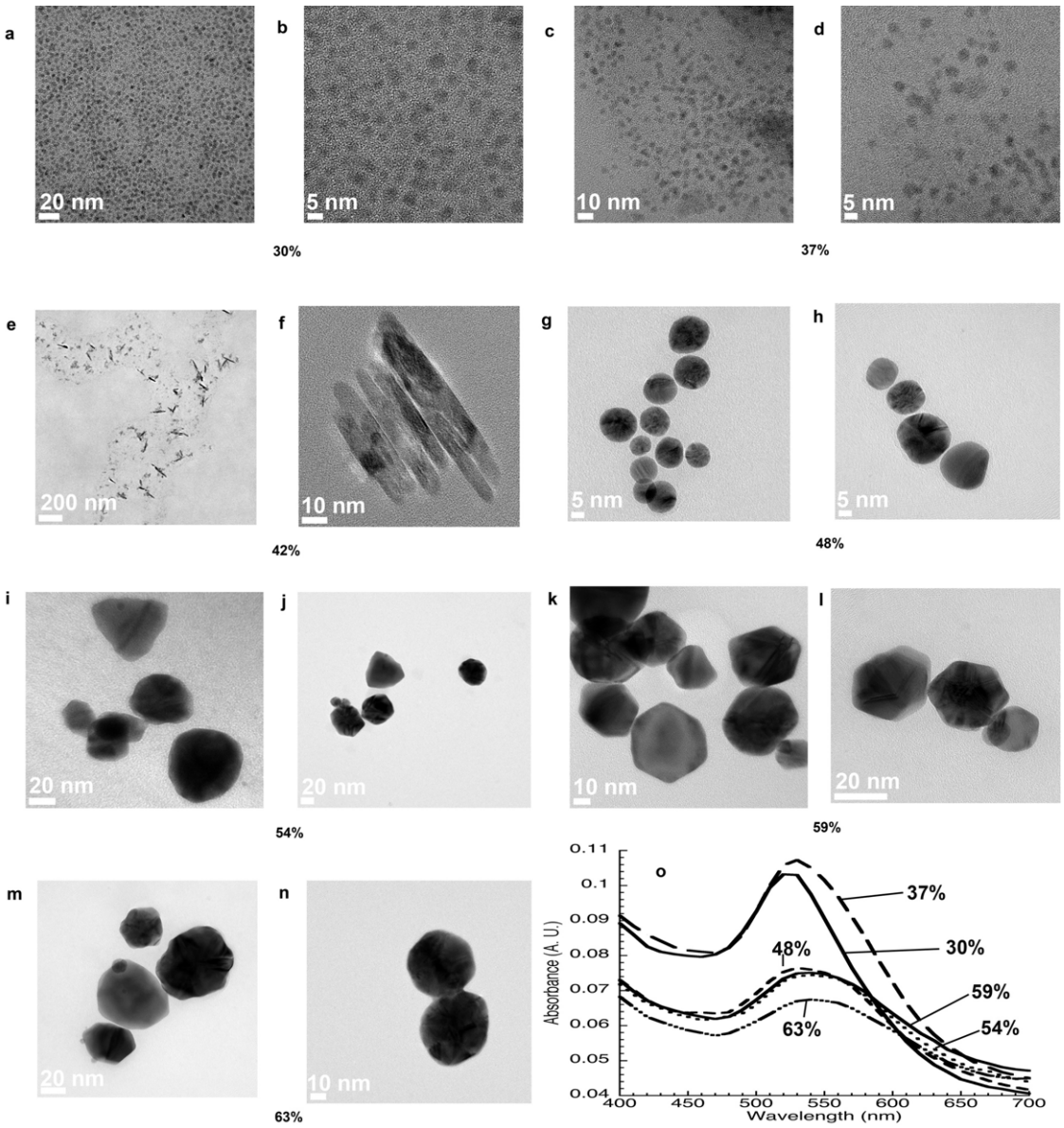

Figure 4. TEM images obtained from different fractions (0.1 ml) collected after sucrose density gradient of the mixture of gold nanoparticles. (a), (b) fraction number 1, at 30% (spherical particles between 2 and 5 nm). (c), (d) fraction number 7, at 37% (spherical particles between 5 and 11 nm). (e), (f) fraction number 12, at 42% (rods, 12–15 nm long and 7–8 nm wide). (g), (h) fraction number 18, at 48% (spherical particles between the size 14 and 20 nm). (i), (j) fraction number 24, at 54% (spherical and triangular particles between 20 and 35 nm). (k), (l) fraction number 29, at 59% (hexagonal particles between 30 and 40 nm). (m), (n) fraction number 33, at 63% (spherical particles between 50 and 70 nm). (o) Absorbance spectra of labeled fractions. Insufficient particles were collected from the 42% fraction to obtain a spectrum.

spectra showed the presence of a surface plasmon resonance (SPR) band centered at 540 nm as shown in figure 1(a) suggesting the presence of Au nanoparticles. Figure 1(b) shows the dynamic light-scattering (DLS) measurements of the mixture indicating the presence of particles in the size range from 2 to 70 nm. X-ray diffraction (XRD) analysis of a droplet of the mixture on a silica substrate showed intense peaks at (111), (200), (220) and (311) Bragg reflections in the 2θ range 30°–80° as shown in figure 1(c); these agree with values reported for gold nanocrystals [29].

Transmission electron microscopy (TEM) images showed a large number of polydisperse particles as shown in figure 2(a). The selected-area electron diffraction (SAED) pattern showed that the particles were crystalline in nature (figure 2(b)). The hexagonal nature of the diffraction spots indicated that the particles were highly oriented (111) with the top normal to the electron beam. The spots could be indexed based on the face-centered-cubic (f.c.c.) structure of gold.

Closer inspection of the particle morphology revealed rods (figures 2(c), (d)), triangles (figures 2(e), (f)), hexagons (figures 2(g), (h)) and stars (figures 2(i), (j)). Among 350 particles from a single TEM image, 44% were spherical, 30% triangular, 12% rod-shaped, 7% hexagonal, 5% pyramidal, and 2% star-shaped as shown in supplementary data (figure S1

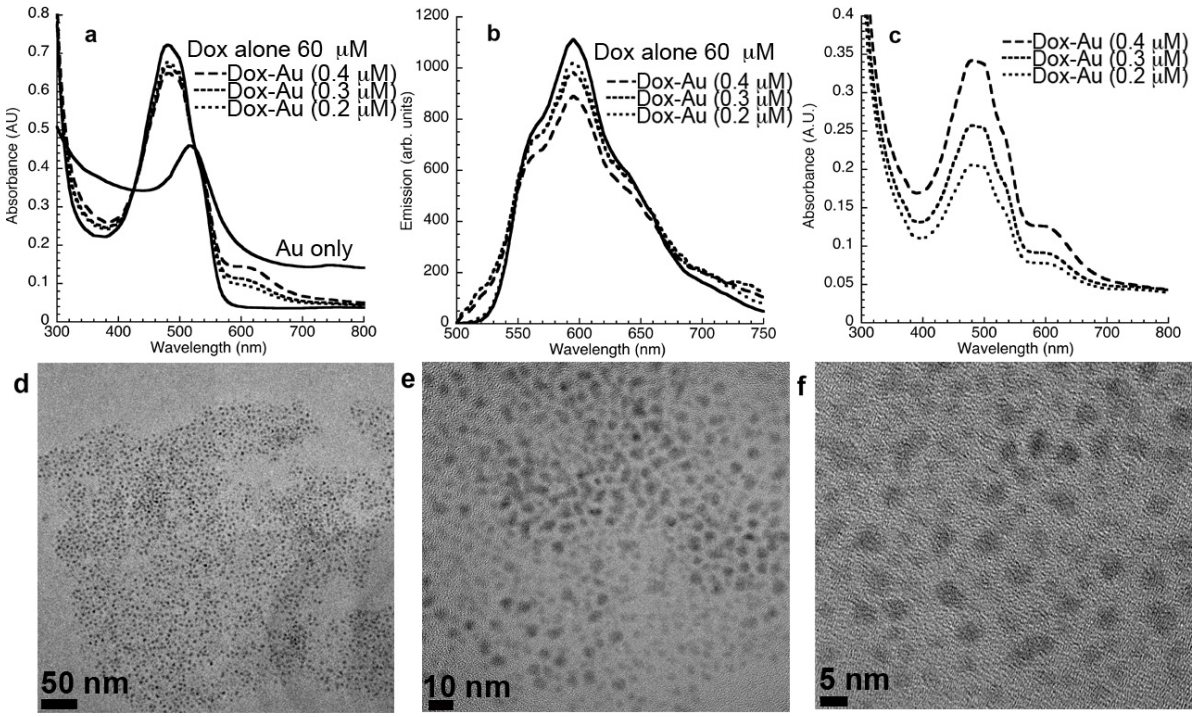

Figure 5. Characterization of Au–doxorubicin conjugates. (a) UV–vis spectra of Au nanoparticles (concentrations 0, 0.2, 0.3 and 0.4 μM) exposed to 60 μM doxorubicin without dialysis to establish effect on spectrum. The spectrum of 0.25 μM Au particles alone is shown for comparison. (b) Fluorescence emission spectra of the samples in (a) upon excitation at 450 nm. (c) Absorbance spectra after dialysis, showing Dox: Au concentrations of 70–80 Dox/Au. (d)–(f) TEM images of the conjugates at increasing magnification showing excellent dispersion.

available at stacks.iop.org/Nano/19/495101). While the spherical particles were polydisperse in the size range from 2 to 70 nm, the other shapes were fairly heterogeneous: the rods averaged 13 ± 1 nm long and 7 ± 1 nm wide ($n = 39$, range 12–15 nm), the hexagons 36 ± 5 nm in diameter ($n = 36$, range 30–42 nm), and the triangles 33 ± 6 nm on a side ($n = 45$, range 25–40 nm). The triangular particles were equilateral, flat and with truncated vertices, features generally observed for triangular silver [23] and gold nanoprisms [31] made by chemical/photochemical methods.

Atomic force microscopy (AFM) showed well-dispersed, heterogeneously shaped nanoparticles (figure 3(a)) with thickness ranging from 3 to 70 nm (figure 3(b)). The surface plot of one of the triangular nanoparticles showed that it had a surface distance of 35.8 nm and vertical distance of 0. 224 nm (figure 3(c)). The surface plot of a pentagon was also carried out on all five edges; the particle had an average surface distance of 41 nm and edge length of 0.307 nm as shown in supplementary data (figure S2 available at stacks.iop.org/Nano/19/495101). The particles dispersed well on the mica surface, demonstrating a hydrophilic surface coat.

We were able to separate the nanoparticles based on their size and shape by a density gradient of 30%–70% sucrose. Fractions of 0.1 ml were collected and monitored for separation by TEM as shown in figure 4. Spheres from 2 to 5 nm concentrated in the 30% fraction (figures 4(a), (b)); spheres from 5 to 11 nm in the 37% fraction (figures 4(c), (d)); rods in the 42% fraction (figures 4(e), (f)); spheres from 14 to 20 nm in 48% (figures 4(g), (h)); spheres and triangles from 20 to 35 nm in 54% (figures 4(i), (j)); pentagons (30–40 nm) in 59% (figures 4(k), (l)); and the largest spheres (50–70 nm) in 63% (figures 4(m), (n); supplementary figures S3, S4 available at stacks.iop.org/Nano/19/495101).

Conjugation of the particles to doxorubicin (Dox) led to a small decrease in the absorbance at peak of the drug and a shift of the plasmon peak to ~615 nm (figure 5(a)). This reduction of the primary absorbance peak has been seen with binding of Dox to other conjugates such as dextran [22]. A modest quenching of Dox fluorescence, proportional to the number of Au particles, was also seen (figure 5(b)). After removal of excess Dox by dialysis, the ratio of Dox to Au was consistently 70–80 Dox/particle (figure 5(c)). Although the plasmon shift suggested there may have be aggregation, TEM analysis revealed that the conjugated particles remained well-dispersed (figures 5(d)–(f)). This peak shift was probably a result of pH due to the highly acidic nature of Dox and its interaction with the Au surface [45]. The conjugates appeared bright under reflectance microscopy at 543 nm; the conjugates alone could also be visualized by reflectance, although they were more readily observed under fluorescence in the doxorubicin channel (supplementary figure S5 available at stacks.iop.org/Nano/19/495101).

The labeling pattern of Au–Dox in HEK293 cells was very different from that seen with Dox alone. With epifluorescence microscopy it could be seen that the drug alone primary concentrated in the nucleus, where it was red, with some green seen outside the cell due to the dependence of the fluorescence on pH and dielectric constant of the medium [24] (figure 6(a)). In contrast, Au–Dox was not seen to enter

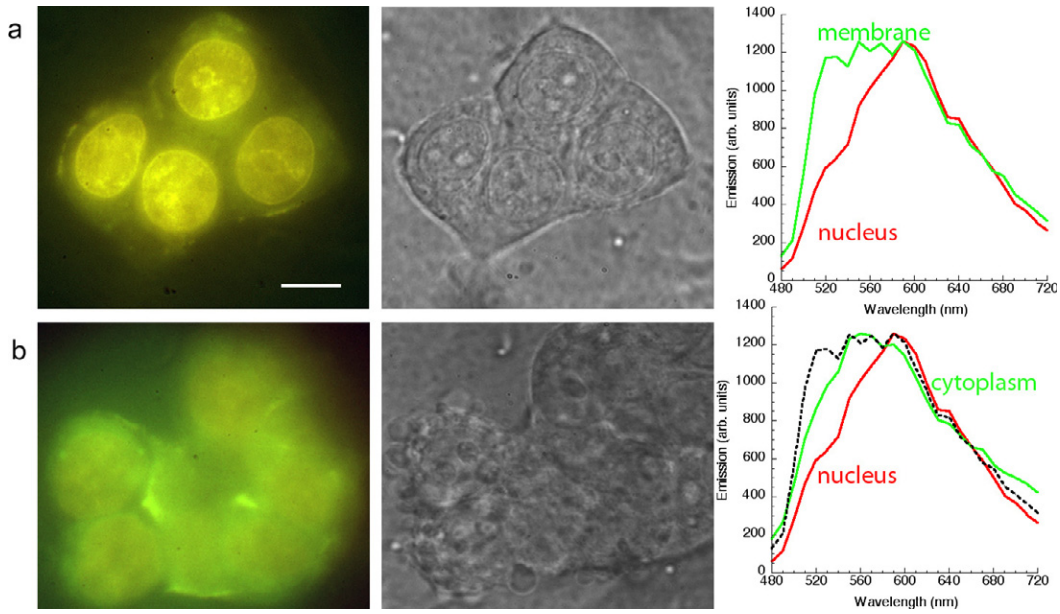

Figure 6. Real-color epifluorescence images and spectra of HEK293 cells exposed to Dox alone (a) and Au–Dox (b). Scale bar = 10 μm for all panels. The cells were excited at 400–450 nm and spectra taken from 480–720 nm in 10 nm increments; all spectra are normalized in the graphs, but the visible images were taken under comparable conditions. (a) In Dox-only cells most fluorescence appears in the nucleus, and cells under phase contrast appear smooth-edged and healthy. The nucleus shows a broad red fluorescence (peak at 600 nm) whereas the small amount of membrane-associated fluorescence has a green-shifted component. (b) In cells with Au–Dox, the cells appear more uniformly bright, and phase-contrast imaging reveals membrane damage in the form of blebbing. The cytoplasmic fluorescence is greener than that of the nucleus, but less broad than that of membrane-associated Dox alone (shown as dashed line).

the nucleus and showed bright fluorescence throughout the cytoplasm (figure 6(b)). Evidence of toxicity in the form of membrane blebbing could be seen with phase contrast; it was found with Au–Dox but not Dox alone (figure 6). Similar membrane-limited toxicity has also been seen with Dox conjugates to the protein transferrin [3].

Assimilated Au particles could be observed with reflectance and fluorescence confocal microscopy (figure 7), which allowed for examination beyond the cell surface. This further reinforced the differences between the doxorubicin alone and Au–Dox labeling. Dox alone concentrated in the cell nucleus, while Au–Dox was essentially excluded from the nucleus and appeared to be associated with intracellular membranous organelles (figures 7(a), (b)). Lysosomal areas of Au–Dox cells showed much greater Dox fluorescence than Au particle scattering, suggesting that Dox may be liberated from the particles in these organelles (figure 7(c)). Brightfield (7(d)) and high power (7(e)) images confirmed these patterns.

The MTT assay measures mitochondrial dehydrogenase activity, and is used as a measure of cell proliferation [19]. With this assay, we found that Au nanoparticles alone did not significantly affect HEK293 cells. Au–Dox showed toxicity per mole of Au comparable to approximately 100-fold greater concentration of free Dox. At Dox/particle ratios of ∼70–80 (see figure 5), this made the conjugates essentially equivalent in toxicity to equal amounts of free Dox (figure 8).

4. Conclusion

Living cells are the best examples of machines that operate at the nanoscale, performing functions ranging from generation of energy to extraction of targeted materials with very high efficiency. Here we set out to explore the feasibility of synthesizing and separating morphologically diverse Au nanoparticles using methods that are more eco-friendly, simpler and more energy-conserving than chemical synthesis. This is an important step toward the use of these diverse shapes in many biological applications and devices, especially wet devices where the hydrophilic surface coat of the particles will be an asset. The detailed mechanism for the formation of a multi-shaped nanocrystals, and the precise makeup of the protein coat, are currently being investigated. This will allow for purification of the enzymes responsible for the synthesis and thus the development of cell-free synthesis methods that will lend themselves to large-scale production of particles without hazardous chemical waste. It may also permit the controlled synthesis of specific sizes and/or shapes, obviating the need for purification.

In comparison with other separation techniques such as centrifugation, capillary electrophoresis [30], electrophoresis [15], chromatography [20], diafiltration [41], sucrose density gradient separation is advantageous as it is simpler, easier to carry out, and takes less time.

The resulting particles are hydrophilic and show little aggregation, even when conjugated to somewhat hydrophobic molecules such as doxorubicin. This is significant because the hydrophobicity of many anti-cancer drugs is a barrier to their effective use. The molecules must be dissolved in toxic solvents to deliver them to cells, and they penetrate less deeply into tissues than is desired. As a result, many encapsulated and conjugated nanoparticle preparations have been prepared to increase the solubility of these agents (for a review, see [7]).

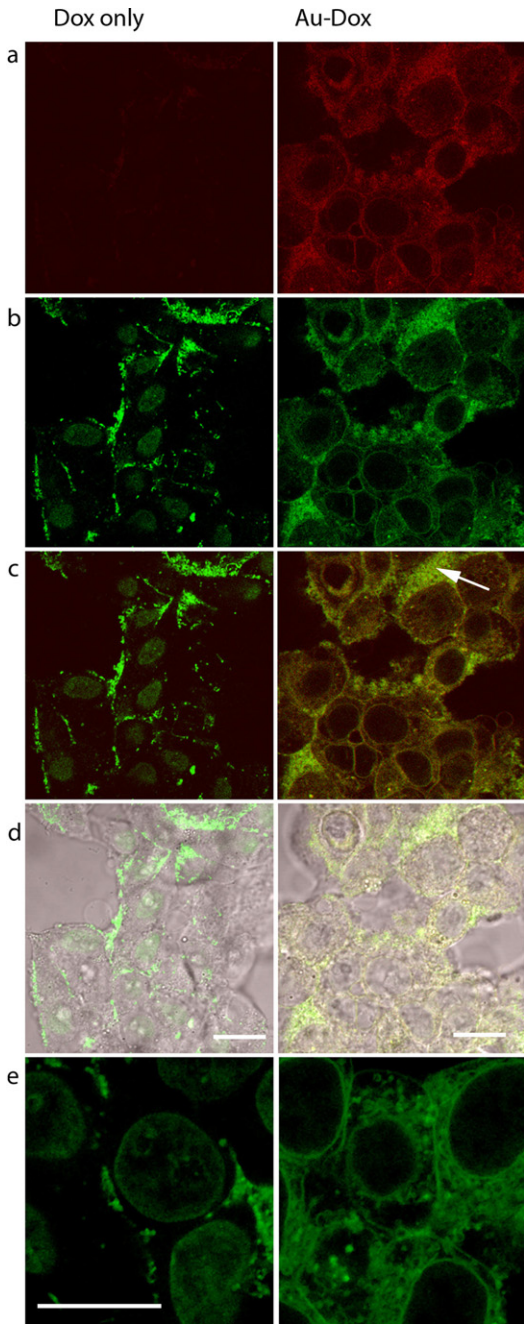

Figure 7. Pseudocolor confocal images of doxorubicin alone (Dox) and Au–Dox in HEK293 cells. Scale bar = 10 μm for all panels. Images show a single 1 μm thick slice through the interior of the cell; the outer membrane cannot be seen. (a) The reflectance image is shown in the red channel, showing little scattering from control cells under these conditions. (b) Dox fluorescence (560 nm longpass) is shown in the green channel. Note the increased brightness in the Au–Dox cells. (c) Overlay of the red and green channels. Note some areas in Au–Dox cells that show a great deal of Dox fluorescence without a corresponding particle signal (arrow). (d) Overlay of the red and green channels and d.i.c. image. (e) Higher magnification image showing detail of nuclear labeling in control cells and cytoplasmic labeling in Au–Dox cells.

Preliminary experiments with cellular uptake reveal efficient assimilation of Au–Dox conjugates prepared by this method and cytotoxicity comparable to that of free Dox.

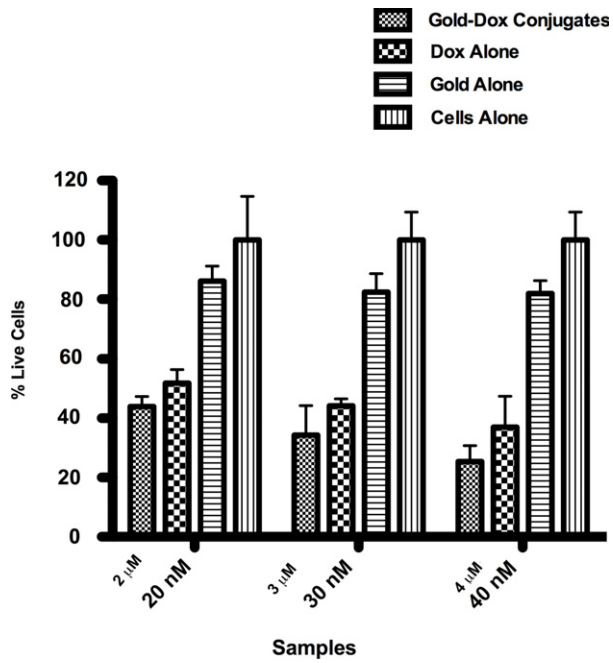

Figure 8. Results of MTT assay for 3 different concentrations of Au–Dox compared with the same molar concentration of Au alone and 100-fold greater concentrations of free Dox. Error bars show the standard deviation of 3 experiments with 8 duplicates per experiment. The percentage of live cells was normalized to the cells-only control. There were no statistically significant differences between cells alone and cells with Au particles in any column, nor any significant differences between Au–Dox and free Dox. The differences between the Au–Dox and Dox columns and the cells-only and Au-only were significant ($p < 0.001$).

The conjugates remain cytoplasmic, however, which may compromise the genotoxicity of the drug [46], an issue which remains to be tested. However, the full extent of cytoplasmic and nuclear targets of doxorubicin is unknown [37]. Future studies will determine the potential usefulness of these conjugates as anti-cancer agents.

Acknowledgments

We thank Mr Thierry Maris and Mr Jean-Philippe Masse for assistance in doing XRD and TEM respectively at École Polytechnique de Montreal, Montreal, Canada, and Patricia Moraille for doing AFM at the Laboratoire de caractérisation, Université de Montréal, Montréal, Canada. This work was supported by NSERC Strategic Grant 336830 2006 and a CIHR Regenerative Medicine and Nanomedicine Team Grant.

References

[1] Alivisatos A P 1996 Perspectives on the physical chemistry of semiconductor nanocrystals *J. Phys. Chem.* **100** 13226–39
[2] Bagalkot V, Zhang L, Levy-Nissenbaum E, Jon S, Kantoff P W, Langer R and Farokhzad O C 2007 Quantum dot—Aptamer conjugates for synchronous cancer imaging, therapy, and sensing of drug delivery based on Bi-fluorescence resonance energy transfer *Nano Lett.* **7** 3065–70

[3] Barabas K, Sizensky J A and Faulk W P 1992 Transferrin conjugates of adriamycin are cytotoxic without intercalating nuclear DNA *J. Biol. Chem.* **267** 9437–42

[4] Bhattacharya D and Gupta R K 2005 Nanotechnology and potential of microorganisms *Crit. Rev. Biotechnol.* **25** 199–204

[5] Brown S, Sarikaya M and Johnson E 2000 A genetic analysis of crystal growth *J. Mol. Biol.* **299** 725–35

[6] Chen S H and Carroll D L 2002 Synthesis and characterization of truncated triangular silver nanoplates *Nano Lett.* **2** 1003–7

[7] Cho K, Wang X, Nie S, Chen Z G and Shin D M 2008 Therapeutic nanoparticles for drug delivery in cancer *Clin. Cancer Res.* **14** 1310–6

[8] Courty A, Henry A I, Goubet N and Pileni M P 2007 Large triangular single crystals formed by mild annealing of self-organized silver nanocrystals *Nat. Mater.* **6** 900–7

[9] Dameron C T, Reese R N, Mehra R K, Kortan A R, Carroll P J, Steigerwald M L, Brus L E and Winge D R 1989 Biosynthesis of cadmium–sulfide quantum semiconductor crystallites *Nature* **338** 596–7

[10] El-Sayed M A 2001 Some interesting properties of metals confined in time and nanometer space of different shapes *Acc. Chem. Res.* **34** 257–64

[11] Gericke M and Pinches A 2006 Biological synthesis of metal nanoparticles *Hydrometallurgy* **83** 132–40

[12] Gong J, Zhang Z M, Bai H J and Yang G E 2007 Microbiological synthesis of nanophase PbS by Desulfotomaculum sp *Sci. China Ser.* E **50** 302–7

[13] Guo D D, Wu C H, Li X M, Jiang H, Wang X M and Chen B A 2008 *In vitro* cellular uptake and cytotoxic effect of functionalized nickel nanoparticles on leukemia cancer cells *J. Nanosci. Nanotechnol.* **8** 2301–7

[14] Haiss W, Thanh N T, Aveyard J and Fernig D G 2007 Determination of size and concentration of gold nanoparticles from UV–vis spectra *Anal. Chem.* **79** 4215–21

[15] Hanauer M, Pierrat S, Zins I, Lotz A and Sonnichsen C 2007 Separation of nanoparticles by gel electrophoresis according to size-and shape *Nano Lett.* **7** 2881–5

[16] Hanessian S, Grzyb J A, Cengelli F and Juillerat-Jeanneret L 2008 Synthesis of chemically functionalized superparamagnetic nanoparticles as delivery vectors for chemotherapeutic drugs *Bioorg. Med. Chem.* **16** 2921–31

[17] Hao E C, Kelly K L, Hupp J T and Schatz G C 2002 Synthesis of silver nanodisks using polystyrene mesospheres as templates *J. Am. Chem. Soc.* **124** 15182–3

[18] Hardman R 2006 A toxicologic review of quantum dots: Toxicity depends on physicochemical and environmental factors *Environ. Health Perspec.* **114** 165–72

[19] Hayon T, Dvilansky A, Shpilberg O and Nathan I 2003 Appraisal of the MTT-based assay as a useful tool for predicting drug chemosensitivity in leukemia *Leuk Lymphoma* **44** 1957–62

[20] Henglein A 1993 Physicochemical properties of small metal particles in solution —microelectrode reactions, chemisorption, composite metal particles, and the atom-to-metal transition *J. Phys. Chem.* **97** 5457–71

[21] Huff T B, Tong L, Zhao Y, Hansen M N, Cheng J X and Wei A 2007 Hyperthermic effects of gold nanorods on tumor cells *Nanomedicine* **2** 125–32

[22] Janes K A, Fresneau M P, Marazuela A, Fabra A and Alonso M J 2001 Chitosan nanoparticles as delivery systems for doxorubicin *J. Control Release* **73** 255–67

[23] Jin R C, Cao Y W, Mirkin C A, Kelly K L, Schatz G C and Zheng J G 2001 Photoinduced conversion of silver nanospheres to nanoprisms *Science* **294** 1901–3

[24] Karukstis K K, Thompson E H Z, Whiles J A and Rosenfeld R J 1998 Deciphering the fluorescence signature of daunomycin and doxorubicin *Biophys. Chem.* **73** 249–63

[25] Kim D, Park S, Lee J H, Jeong Y Y and Jon S 2007 Antibiofouling polymer-coated gold nanoparticles as a contrast agent for *in vivo* x-ray computed tomography imaging *J. Am. Chem. Soc.* **129** 7661–5

[26] Kostoryz E L and Yourtee D M 2001 Oxidative mutagenesis of doxorubicin-Fe(III) complex *Mutat. Res.* **490** 131–9

[27] Kumar S A, Abyaneh M K, Gosavi S W, Kulkarni S K, Ahmad A and Khan M I 2007 Sulfite reductase-mediated synthesis of gold nanoparticles capped with phytochelatin *Biotechnol. and Appl. Biochem.* **47** 191–5

[28] Kumar S A, Abyaneh M K, Gosavi S W, Kulkarni S K, Pasricha R, Ahmad A and Khan M I 2007 Nitrate reductase-mediated synthesis of silver nanoparticles from $AgNO_3$ *Biotechnol. Lett.* **29** 439–45

[29] Leff D V, Brandt L and Heath J R 1996 Synthesis and characterization of hydrophobic, organically-soluble gold nanocrystals functionalized with primary amines *Langmuir* **12** 4723–30

[30] Liu F K and Wei G T 2004 Adding sodium dodecylsulfate to the running electrolyte enhances the separation of gold nanoparticles by capillary electrophoresis *Anal. Chim. Acta* **510** 77–83

[31] Malikova N, Pastoriza-Santos I, Schierhorn M, Kotov N A and Liz-Marzan L M 2002 Layer-by-layer assembled mixed spherical and planar gold nanoparticles: control of interparticle interactions *Langmuir* **18** 3694–7

[32] Manna L, Scher E C and Alivisatos A P 2000 Synthesis of soluble and processable rod-, arrow-, teardrop-, and tetrapod-shaped CdSe nanocrystals *J. Am. Chem. Soc.* **122** 12700–6

[33] Medintz I L, Uyeda H T, Goldman E R and Mattoussi H 2005 Quantum dot bioconjugates for imaging, labelling and sensing *Nat. Mater.* **4** 435–46

[34] Patil R R, Guhagarkar S A and Devarajan P V 2008 Engineered nanocarriers of doxorubicin: a current update *Crit. Rev. Ther. Drug Carrier Syst.* **25** 1–61

[35] Peng X G, Manna L, Yang W D, Wickham J, Scher E, Kadavanich A and Alivisatos A P 2000 Shape control of CdSe nanocrystals *Nature* **404** 59–61

[36] Pintoalphandary H, Balland O and Couvreur P 1995 A new method to isolate polyalkylcyanoacrylate nanoparticle preparations *J. Drug Target.* **3** 167–9

[37] Serafino A, Sinibaldi-Vallebona P, Pierimarchi P, Bernard P, Gaudiano G, Massa C, Rasi G and Ranagnan G 1999 Induction of apoptosis in neoplastic cells by anthracycline antitumor drugs: nuclear and cytoplasmic triggering? *Anticancer Res.* **19** 1909–18

[38] Shankar S S, Rai A, Ankamwar B, Singh A, Ahmad A and Sastry M 2004 Biological synthesis of triangular gold nanoprisms *Nat. Mater.* **3** 482–8

[39] Sun Y G, Mayers B and Xia Y N 2003 Transformation of silver nanospheres into nanobelts and triangular nanoplates through a thermal process *Nano Lett.* **3** 675–9

[40] Sweeney R Y, Mao C B, Gao X X, Burt J L, Belcher A M, Georgiou G and Iverson B L 2004 Bacterial biosynthesis of cadmium sulfide nanocrystals *Chem. Biol.* **11** 1553–9

[41] Sweeney S F, Woehrle G H and Hutchison J E 2006 Rapid purification and size separation of gold nanoparticles via diafiltration *J. Am. Chem. Soc.* **128** 3190–7

[42] Visaria R K, Griffin R J, Williams B W, Ebbini E S, Paciotti G F, Song C W and Bischof J C 2006 Enhancement of tumor thermal therapy using gold nanoparticle-assisted tumor necrosis factor-alpha delivery *Mol. Cancer Ther.* **5** 1014–20

[43] Wang X M *et al* 2007 The application of Fe_3O_4 nanoparticles in cancer research: a new strategy to inhibit drug resistance *J. Biomed. Mater. Res.* A **80** 852–60
[44] Yin Y and Alivisatos A P 2005 Colloidal nanocrystal synthesis and the organic–inorganic interface *Nature* **437** 664–70
[45] Yokoyama K and Welchons D R 2007 The conjugation of amyloid beta protein on the gold colloidal nanoparticles' surfaces *Nanotechnology* **18** 105101–7
[46] You J, Hu F, Du Y and Yuan H 2008 Improved cytotoxicity of doxorubicin by enhancing its nuclear delivery mediated via nanosized micelles *Nanotechnology* **19** 255103–11